

# Numerical Modeling and Analysis of Flexure-Pivot Tilting-Pad Bearing

**Junho Suh**  
Mem. ASME

School of Mechanical Engineering,  
Pusan National University,  
Busan 46241, South Korea  
e-mail: junhosuh@pusan.ac.kr

**Alan Palazzolo**  
Fellow ASME

Department of Mechanical Engineering,  
Texas A&M University,  
College Station, TX 77840  
e-mail: a-palazzolo@tamu.edu

**Yeon-Sun Choi**

Department of Mechanical Engineering,  
Sungkyunkwan University,  
Suwon 16419, South Korea  
e-mail: yschoi@yurim.skku.ac.kr

*This paper presents a new approach for modeling flexure-pivot journal bearings (FPJB) employing a three-dimensional (3D) elasto-hydro-dynamic (EHD) lubrication model. The finite element (FE) method is adopted for an analysis of the (1) pad-pivot dynamic behavior and the (2) fluid force. The isoviscosity Reynolds equation is utilized to calculate the fluid force acting on a flexure-pivot pad bearing and spinning journal. Computational efficiency is achieved utilizing modal coordinate transformation for the flexible pad-pivot dynamic analysis. Fluid film thickness plays a critical role in the solution of Reynolds equation and is evaluated on a node-by-node basis accounting for the pad and web deflections. The increased fidelity of the novel modeling approach provides rotating machinery designers with a more effective tool to analyze and predict rotor-bearing dynamic behavior. [DOI: 10.1115/1.4036275]*

## 1 Introduction

Tilting pad journal bearings (TPJBs) provide superior stability characteristics in a rotor-bearing dynamic system by reducing cross-coupled dynamic stiffness and have been widely used to achieve the goal of higher-speed and increased power. Flexure-pivot journal bearings (FPJBs) provide similar rotordynamic performance to a TPJB and eliminate some of its weaknesses such as a tight manufacturing tolerance, radial pivot deformation, and pivot wear, which may lead to reduced rotordynamic performance. FPJBs also have smaller size, simpler design and manufacturing processes, and very low manufacturing error as compared with a TPJB. Tilting motions of a TPJB and a FPJB are depicted in Figs. 1(a) and 1(b), respectively. The TPJB provides pad tilt motion around a pivot contact line or point depending on the pivot configuration, whereas the FPJB's tilt motion results from its elastic deformations. Elastic deformations of the pivot and pad are known to have an influence on the bearing static and dynamic characteristics. The effects of FPJB flexibility on dynamic coefficients are studied here where the literature almost solely focuses on the effect of TPJB pad and pivot flexibility.

**1.1 Titling Pad Journal Bearing.** Lund [1] presented a numerical approach to calculate bearing direct and cross-coupled coefficients of a TPJB. Harmonic rotor motion was assumed so that synchronous frequency reduced bearing coefficients were determined. This is the first publication regarding the frequency reduced TPJB dynamic coefficients. Nilsson [2] extended Lund's research [1] presenting the influence of bearing pad flexibility on the dynamic coefficients. Bearing pad flexibility produced a dramatic change in dynamic performance but relatively small change in static capacity. The pad flexibility was found to influence damping coefficients more than stiffness coefficients. Lund and Pedersen [3] presented a finite difference-based perturbation solution of Reynolds equation taking into account both pad flexibility and pivot stiffness. Fluid film clearance change under lubricant pressure was calculated with the assumption that the bearing pad behaves similar to an analytical beam model resulting in reduced computation time. The amount of the pad deformation was characterized by a change in beam curvature.

Earles et al. [4] developed a two-dimensional finite element (FE) pad model to calculate the elastic deformation under the fluid

pressure; however, the deformation was reduced to a single-degree-of-freedom, the radius of curvature. The isoviscous Reynolds equation was solved, and synchronously reduced dynamic coefficients were provided. The first numerical model for the three-dimensional (3D) pad elastic deformation was developed by Desbordes et al. [5] and bearing dynamic behavior under various unbalance eccentricities was evaluated. Pad deformation was evaluated by use of a static load approach. Nodes on the pivot line were constrained and additional nodes around the pivot location were fixed to produce the pad tilt motion and avoid a singular matrix problem.

**1.2 Flexure Pivot Journal Bearing.** Armentrout and Paquette [6] introduced the first research paper about FPJB numerical modeling in 1993. Variations of the dynamic coefficients with the varying web thickness and the equivalent pad tilt stiffness were provided. At a thick web (high tilt stiffness), the FPJB exhibited increased cross-coupled terms as in the fixed pad bearing. Dynamic behavior of the web was assumed to produce only pad tilt motion represented by a rotational spring attached to the rigid pad at the pivot location. Chen [7] presented a method for the evaluation of the FPJB force coefficients. Rotational, radial, and circumferential web stiffness formulae were provided where the web is considered as a simplified beam model. The pad assembly method was adopted with the coordinate transformation between the fixed local and the global coordinates. The pads were assumed to be rigid, and the support web was represented by means of a spring attached to a point pivot.

Both predicted and experimental results were provided by San Andrés and Walton [8,9] In the numerical model, the web was assumed to produce only rotational stiffness [8], which is the same approach presented by Armentrout and Paquette [6]. Turbulent bulk flow was used to evaluate the fluid pressure acting on the bearing pad, and the thermal effects were taken into account. Experimental results of static loading characteristics of four-pads FPJB subjected to various running conditions were provided. Bearing eccentricity, pad temperature, and power losses were measured and compared to numerical predictions [9]. Al-Ghasem and Childs [10] presented test results of load on pad FPJB configuration and predicted results. Both isoviscosity Reynolds equation and bulk-flow Navier-Stokes models were utilized for the numerical analysis. Whirl frequency ratio was found to decrease with increased load and increase with increased rotor spin speed. Rodriguez and Childs [11] measured dynamic coefficients of a load on pad FPJB, and found that the real parts of the direct

Contributed by the Tribology Division of ASME for publication in the JOURNAL OF TRIBOLOGY. Manuscript received September 5, 2015; final manuscript received March 3, 2017; published online May 26, 2017. Assoc. Editor: Mihai Arghir.

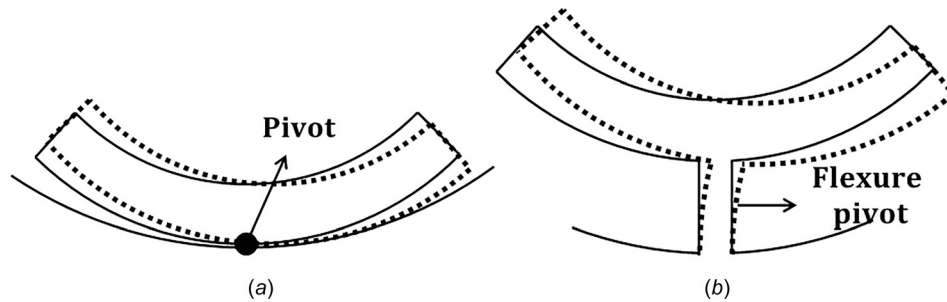


Fig. 1 Tilting motion around pivot: (a) Tilting pad bearing and (b) flexure pivot bearing

stiffness terms are quadratic functions of the excitation frequency. Their numerical results underestimated the added mass coefficients for the full excitation frequencies. Hensley and Childs [12] measured FPJB dynamic coefficients using a hydraulic shaker exciting the bearing stator as in Refs. [10] and [11]. A pseudorandom excitation method was adopted for the force coefficients over a broad frequency range. Direct added mass was required to account for the measured frequency-dependent dynamic coefficient.

A flexible pad-web model was first provided by Kepple et al. [13] and the web stress under the static and dynamic fluid load was simulated. Furthermore, fatigue life prediction was carried out utilizing modified Goodman diagram incorporating a commercial FE solver. However, the bearing static and dynamic performance was not predicted since the numerical model was limited to a single pad-web model. Pettinato and De Choudhury [14] carried out both rotordynamic tests and theoretical analysis of the FPJB, where both synchronous and nonsynchronous dynamic performances were measured and compared. Frequency-dependent bearing characteristics were strongly observed with their bearing model.

**1.3 Modal Reduction Method.** A single component, combined web-pad, 3D dynamic FE model is employed for evaluation of the FPJB static and dynamic performance. Accurate representation of the pad elastic deformations requires many degrees-of-freedom resulting in high computation issue. Furthermore, the transient dynamic solver is utilized for the pad-web and journal system to integrate all the way to steady-state conditions. For the elasto-hydro-dynamic (EHD) lubrication modeling, several approaches have been developed to improve the computational efficiency. Thermo-elasto-hydro-dynamic (TEHD) TPJB modeling method was treated by Kim et al. [15] utilizing a modal reduction approach to efficiently calculate the TPJB elastic deformation. Synchronous dynamic coefficients were determined and compared with experimental results. Thermal expansion of the pad and spinning journal caused a significant effect on the TPJB characteristics.

Similarly, Boedo and Booker [16] also made remarkable contributions on the EHD lubrication model. A journal bearing in a connecting rod, which connects a piston to the crankshaft in a reciprocating piston engine, was simulated with the consideration of mass conservation, surface roughness, and structural inertia effects. Elastic deformation of the bearing was found to be represented by linear combination of only a few modes even with the consideration of the body forces and the surface roughness. Boedo and Booker [17–20] extended their numerical approach with the utilization of the mode-based EHD lubrication model.

Suh and Palazzolo [21] presented a numerical model for the TEHD TPJB, where both pad thermal and elastic deformation were taken into account employing a 3D FE model. Nonlinear time transient analysis of the system was performed to avoid the singular matrix problem that arises in a gradient search approach, due to rigid body tilt motions of the 3D flexible pad, FE model. Hertzian contact theory was adopted for the pivot

stiffness calculation. A modal coordinate transformation was performed to reduce the computation time. The related, former research on flexible pad FE models did not provide the film thickness formula for an arbitrary pad thermal and elastic deformation. Similarly, only the first bending mode and rigid body pad tilting motion were employed to determine the static and dynamic behavior of the TPJB. The change in bearing preload due to the elastic and thermal deformation was investigated and found to have significant effects on the TPJB dynamic characteristics.

Earlier studies of FPJB dynamic characteristics utilized a model consisting of a rigid pad and concentrated rotational, radial, and tangential springs applied at the pivot location. The present approach utilizes a fully flexible, single domain, pad-pivot FE model, where the pad and pivot deform together as a single body, which provides a more accurate model for predicting dynamic behavior.

## 2 Numerical Modeling

**2.1 Flexible Pad-Pivot Dynamic Model.** One of the unique contributions of this research is the utilization of the FE method for the analysis of both flexible pad and pivot. Earlier studies have utilized “equivalent” rotational, radial, and tangential pivot stiffness based on the web length and thicknesses instead of employing a complete flexible web structure since a considerable amount of degrees of freedom is required for modeling the pivot dynamic motion [6–8]. Figure 2 shows 3D flexible pad-pivot dynamic FE model. The bearing housing is assumed to be rigid so that the end of the web is fixed. Three-dimensional, elastic, eight-node isoparametric element is utilized to divide the model domain. The equation of motion for the pad-pivot dynamic analysis is described in Eq. (1), where the pad-pivot nodal mass and stiffness are taken into account. Internal damping of the structure is not considered and  $X_{E,PW}$  indicates the pad-pivot nodal displacement vector. Each node has three degrees-of-freedom in  $x$ ,  $y$ , and  $z$  directions.  $F_{E,PW-FL}$  is a fluid load applied on the pad top surface, where the fluid force is calculated by Reynolds equation [22].

An iteration scheme composed of perturbation loops such as the Newton–Raphson method produced divergence problems especially for the heavy load case. A nonlinear time transient dynamic solver was suggested by Suh and Palazzolo [21] to avoid the divergence problems. Nonlinear time transient journal and pad-pivot dynamic analysis are performed, solving the equations of motion for the spinning journal and elastic pad-pivot motions simultaneously. The Runge–Kutta numerical integration scheme is adopted. The spinning rotor is placed in the center of bearing pads initially for the FPJB and spinning journal to reach the static equilibrium conditions. In the transient dynamic solver, the spinning journal and flexible pad-pivot reach steady state until the pad-pivot and journal degrees-of-freedom do not produce any time varying displacement and velocity. A detailed algorithm for the transient dynamic analysis and static equilibrium analysis will be discussed in Sec. 2.4.

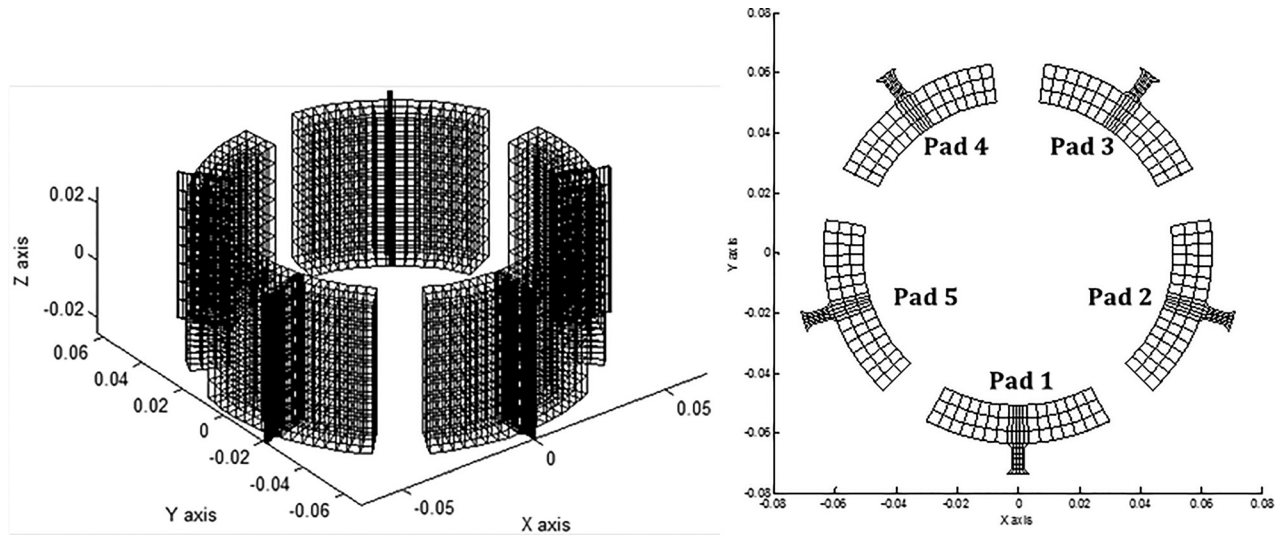


**Fig. 2 Three-dimensional flexible pad-pivot dynamic FE model**

The nonlinear transient simulation of the flexible pad-pivot and rotor dynamic model may require excessive computation time arising from the degrees-of-freedom of the pad-pivot FE model. If the pad-pivot dynamic behavior can be expressed in terms of selected governing eigenmodes, efficient computing can be achieved with the dramatically reduced degrees-of-freedom. This study assumes that a good selection of pad-pivot eigenmodes provides an accurate prediction of rotordynamic behavior. Low frequency-based eigenmodes selection is performed in this research [21]. The number of modes for the accurate prediction of the FPJB dynamic behavior will be discussed in Sec. 3.2.

The pad-pivot elastic deformation vector  $X_{E,PW}$  can be expressed in terms of modal displacement vector ( $Z_{E,PW}$ ) and eigenvectors ( $\Phi_{E,PW}$ ) as shown in Eq. (2). In accordance with the relationship between modal and physical coordinates, the pad-pivot equation of motion shown in Eq. (2) can be decoupled utilizing modal orthogonality as shown in Eqs. (3) and (4)

$$M_{E,PW}\ddot{X}_{E,PW} + K_{E,PW}X_{E,PW} = F_{E,PW,FL} \quad (1)$$

$$X_{E,PW} = \Phi_{E,PW}Z_{E,PW} \quad (2)$$

$$\Phi_{E,PW}^T M_{E,PW} \Phi_{E,PW} \ddot{Z}_{E,PW} + \Phi_{E,PW}^T K_{E,PW} \Phi_{E,PW} Z_{E,PW} = \Phi_{E,PW}^T F_{E,PW,FL} \quad (3)$$

$$m_{E,PW} \ddot{Z}_{E,PW} + k_{E,PW} Z_{E,PW} = f_{E,PW,FL} \quad (4)$$

**2.2 Film Thickness.** For the evaluation of film thickness of FPJB, earlier studies have considered rigid pad-based analytical method where only rigid body and pad tilting motion are taken into account; however, when it comes to the full flexible pad-pivot model producing an arbitrary pad-pivot deformation under fluid pressure, a node-based new approach is required. This research adopted a node-based film thickness method suggested by Suh and Palazzolo [21]. A schematic diagram for the film thickness ( $h_n$ ) and temporal derivative ( $dh_n/dt$ ) is described in Fig. 3. The film thickness ( $h_n$ ) is distance between two corresponding nodes,  $p_n$  and  $j_n$ .  $p_n$  is the pad top surface node and  $j_n$  is a journal surface node. Nodal position of  $p_n$  can be represented by means of the nodal position defined by  $(x_n, y_n, z_n)$  of the pad-pivot FE model. On the other hands,  $j_n$  cannot be calculated by the nodal position of the shaft because the spinning journal is represented by a single point ( $O_s$ ) as shown in Fig. 3. The distance

between  $p_n$  and  $j_n$  is represented by Eq. (5) and the temporal derivative is Eq. (6), where  $R_n$  is a journal radius

$$h_n = \sqrt{(x_n - x_s)^2 + (y_n - y_s)^2} - R_n \quad (5)$$

$$\frac{dh_n}{dt} = \frac{1}{\sqrt{(x_n - x_s)^2 + (y_n - y_s)^2}} \cdot \left\{ (x_n - x_s) \cdot \left( \frac{dx_n}{dt} - \frac{dx_s}{dt} \right) + (y_n - y_s) \cdot \left( \frac{dy_n}{dt} - \frac{dy_s}{dt} \right) \right\} \quad (6)$$

**2.3 Reynolds Equation.** Reynolds equation is the governing equation to evaluate the fluid pressure developed between two moving surfaces with relative velocities. If the bearing pad provides zero linear velocity in the circumferential direction, the Reynolds equation becomes (7). For the derivation of the Reynolds equation, the following are assumed.

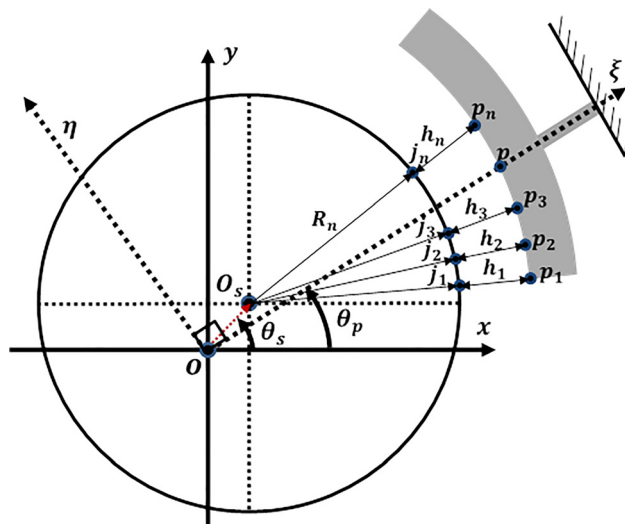


**Fig. 3 Node-based film thickness evaluation**

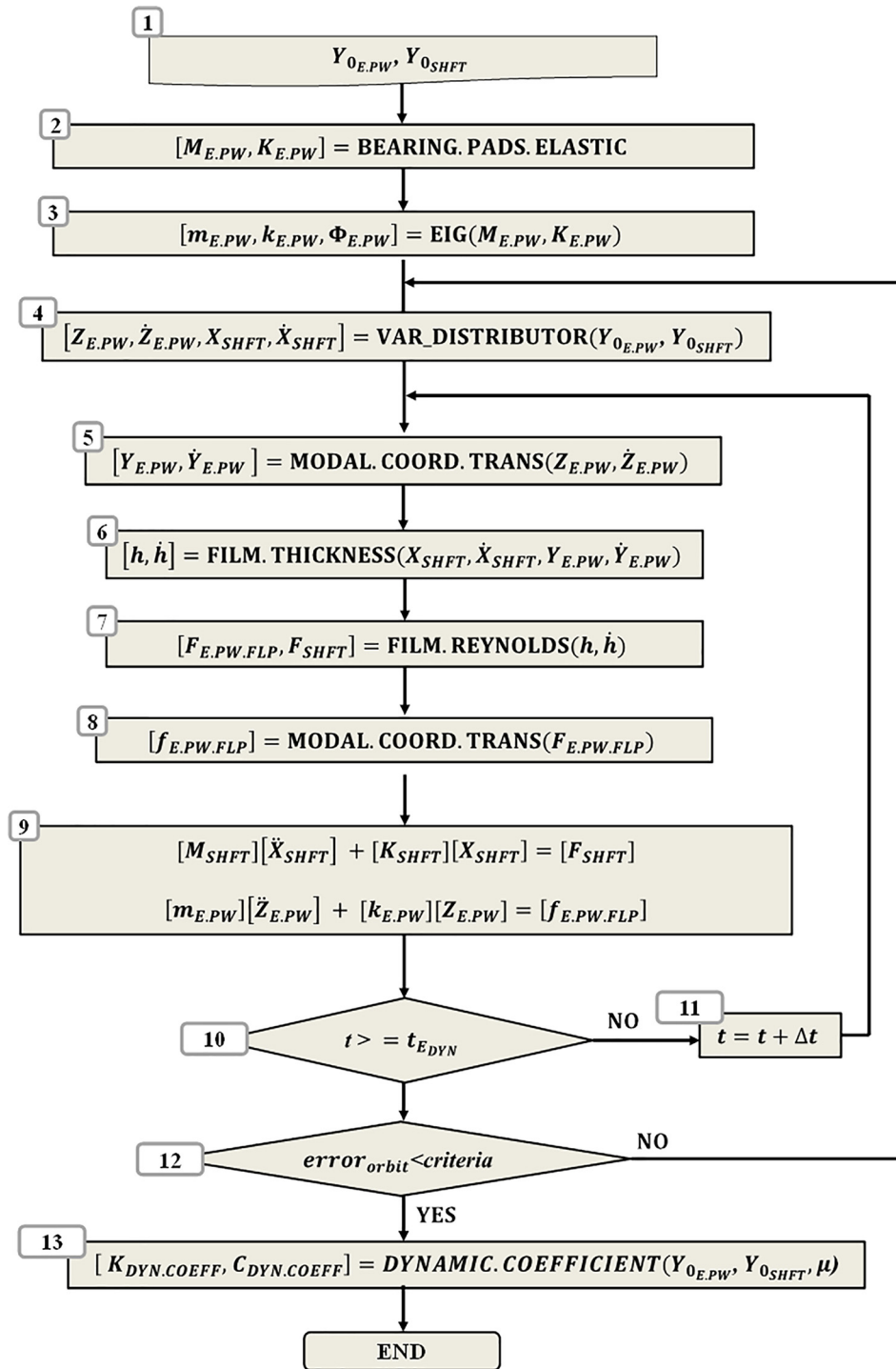


Fig. 4 Algorithm for nonlinear rotor-bearing transient analysis

- (1) Newtonian fluid
- (2) Fluid pressure is constant in the film thickness direction
- (3) Fluid density is constant regardless of pressure
- (4) Thin film produce a laminar flow
- (5) Shaft ovaling effect is not taken into account
- (6) Fluid inertia is neglected.
- (7) Slip at the fluid and solid interface is neglected.
- (8) Reynolds cavitation boundary condition is employed.

$$\nabla \cdot \left( \frac{h^3}{12\mu} \nabla p \right) = (\nabla h) \cdot \mathbf{U} + \frac{\partial h}{\partial t} \quad (7)$$

**2.4 Algorithm.** Pad-pivot elastic deformation caused by the external fluid force is analyzed in the nonlinear transient dynamic solver, where the fluid pressure is updated in accordance with the newly calculated pad film thickness ( $h_n$ ). Most of the process discussed in this section is about the algorithm to produce the static equilibrium condition of the flexible pad-pivot and the spinning journal. A detailed algorithm is depicted in Fig. 4 and is explained as follows:

- (1) The numerical solver begins with the initial states of flexible pad-pivot ( $Y_{0E.PW}$ ) and journal ( $Y_{0SHFT}$ ).
- (2) Mass ( $M_{E.PW}$ ) and stiffness ( $K_{E.PW}$ ) matrices of dynamic pad-pivot FE model is created based on the bearing input

- parameters. Since this research adopted node-based film thickness method, precise pad-pivot geometry should be provided for an accurate prediction of the film clearance.
- (3) For the coordinate transformation between general (modal) and physical coordinates, diagonalized modal mass ( $m_{E,PW}$ ) and modal stiffness ( $k_{E,PW}$ ) should be pre-calculated before the transient dynamic analysis.
  - (4) Initial condition of dynamic solver is composed of pad-pivot state ( $Y_{0E,PW}$ ) in the generalized coordinate and journal state ( $Y_{0SHFT}$ ) in the physical coordinate. They should be delivered to each equation of motion for pad-pivot and shaft.
  - (5) For the evaluation of the film thickness ( $h_n$ ) and its temporal derivative ( $dh_n/dt$ ), the pad-pivot nodal position ( $Z_{E,PW}$ ) and velocity ( $\dot{Z}_{E,PW}$ ) represented in terms of modal coordinate are transformed into the states represented by physical coordinate.
  - (6) For the evaluation of the fluid force utilizing Reynolds equation,  $h_n$  and  $dh_n/dt$  are evaluated by means of physical states of pad-pivot ( $Y_{E,PW}, \dot{Y}_{E,PW}$ ) and journal ( $X_{SHFT}, \dot{X}_{SHFT}$ ).
  - (7) Fluid load ( $F_{E,PW,FLP}$ ) is calculated by the Reynolds equation FE code with the utilization of the precalculated lubricant thickness ( $h_n$ ) and its temporal derivative ( $dh_n/dt$ ).
  - (8) Fluid pressure acting on the bearing pad top surface is transformed into modal force ( $f_{E,PW,FLP}$ ) to be applied into Eq. (4).
  - (9) Pad-pivot and journal transient dynamic solver are executed in the same time domain with zero unbalance force acting on the spinning journal. Force acting on the spinning journal ( $F_{SHFT}$ ) includes fluid pressure and gravity force. MATLAB ODE45 and ODE 15s, adaptive time step numerical integration solvers, are adopted to solve these equations.
  - (10) The whole process from (5) to (10) is performed until  $t \geq t_{E,DYN}$ .
  - (11) Otherwise, the whole process is repeated. Adaptive time step ( $\Delta t$ ) numerical integration solver is performed, and the numerical integration is executed from next time step ( $t = t + \Delta t$ ).
  - (12) In accordance with the final pad-pivot and journal states, frequency reduced bearing dynamic coefficients are calculated [17].

### 3 Simulation Results and Discussions

**3.1 Web Thickness Effect.** The FPJB provides many of beneficial dynamic characteristics coming from the TPJB. Thin web produces the TPJB properties while the thick web provides fixed pad bearing behavior. However, optimum bearing configuration requires a tradeoff between a thin web to avoid instability arising from cross coupled dynamic coefficients and a thick web to maximize the bearing load capability [6].

This section examines the web thickness effects on FPJB static and dynamic behavior. The bearing input parameters for the simulation are presented in Table 1. Fifteen different web thickness models (1–15 mm) are simulated with the rotor spin speed ranging from 5000 rpm to 15,000 rpm. Web length stays constant on all the web thickness models.

Both rigid and flexible pad FPJBs are simulated in this section. Most of the earlier researches about the FPJB have developed rigid tilting pad model constrained by an equivalent rotational spring [7], which is identical to the TPJB except the rotational stiffness. In this research, both rotational and radial stiffness are taken into account in the rigid-pad FPJB model, and the circumferential stiffness is ignored since the load on the pivot in the circumferential direction is assumed to be zero. In the case of the flexible pad-pivot FPJB model, both web and

**Table 1 Bearing simulation parameters**

Lubricant properties	
Viscosity (Pa·s)	0.0203
Density (kg/m <sup>3</sup> )	860
Supply pressure (Pa)	$1.32 \times 10^5$
Bearing pad input parameters	
Load configuration	LOP
Number of pads	5
Pad arc length (deg)	56
Offset	0.5
Radius of shaft (m)	0.0508
Bearing clearance (m)	$7.48 \times 10^{-5}$
Preload	0.5
Bearing length (m)	0.0508
Young's modulus (Pa)	$2.10 \times 10^{11}$
Density (kg/m <sup>3</sup> )	7850
Poisson's ratio	0.3
Bearing load (N)	2100
Web length (m)	$5.0 \times 10^{-3}$
Pad thickness (m)	0.0127
Simulation parameters	
Web thickness (m)	0.001–0.015
Rotor spin speed (rpm)	5000, 10,000, 15,000

pad produce flexibility as seen in Fig. 5. Cross-sectional views of three different web thickness FE models are shown in Fig. 5, where only a two-dimensional view is provided for the readers to see the differences of pad-pivot geometry easily. Twenty eigenmodes of flexible pad-pivot FE model are selected based on the lower eigenvalues [21].

In order to verify the current FPJB numerical model for the first stage, static and dynamic characteristics are calculated and compared to the verified rigid-pad TPJB and rigid fixed-pad bearings. TPJB and fixed-pad bearing have the same bearing input parameters as the FPJB except the flexure-pivot configuration. If the rigid-pad FPJB model has zero pivot tilting stiffness and rigid radial pivot, it will produce the rigid-pad TPJB behavior. The rigid-pad FPJB will provide the fixed pad bearing properties if the rigid tilting and radial stiffness are assumed.

Journal eccentricity ratio and attitude angle with varying web thickness are described in Figs. 6 and 7, respectively. At the thinnest web (1 mm), TPJB static properties are produced regardless of the rotor spin speed. On the other hand, both journal eccentricity ratio and attitude angle converge into the fixed-pad bearing properties as the web thickness increases. At 5000 rpm, static characteristics converge more quickly than at 15,000 rpm as seen in Figs. 6 and 7. Rigid-pad FPJB reaches the fixed-pad bearing properties more quickly than the flexible pad model. Even at 15 mm of the web thickness, flexible pad-pivot model stays in the transient regime between the tilting pad and fixed geometry regime, whereas the rigid-pad model provides almost the fixed pad behavior.

Synchronously reduced stiffness coefficients are shown in Fig. 8, where frequency dependency is ignored. In the case of cross-coupled terms, TPJB properties are produced at the thin web while fixed-pad bearing characteristics are being developed as the web thickness increases. Figures 8(a), 8(b), and 8(c) show  $k_{xx}$  at 5000, 10,000, and 15,000 rpm, respectively. As the web thickness increases,  $k_{xx}$  goes up rapidly in the opposite direction of the fixed-pad bearing properties. After this change, they go down into the fixed-pad bearing regime. At 15 mm of the web thickness, the flexible pad-pivot FPJB FE model still stays in the transient regime, whereas the rigid-pad model produces steady value after 12 mm of the web thickness. Differences between the rigid and flexible pad-pivot models still exist at the thickest web (15 mm). Cross-coupled terms are shown in Figs. 8(g)–8(i). Both  $k_{xy}$  and  $k_{yx}$

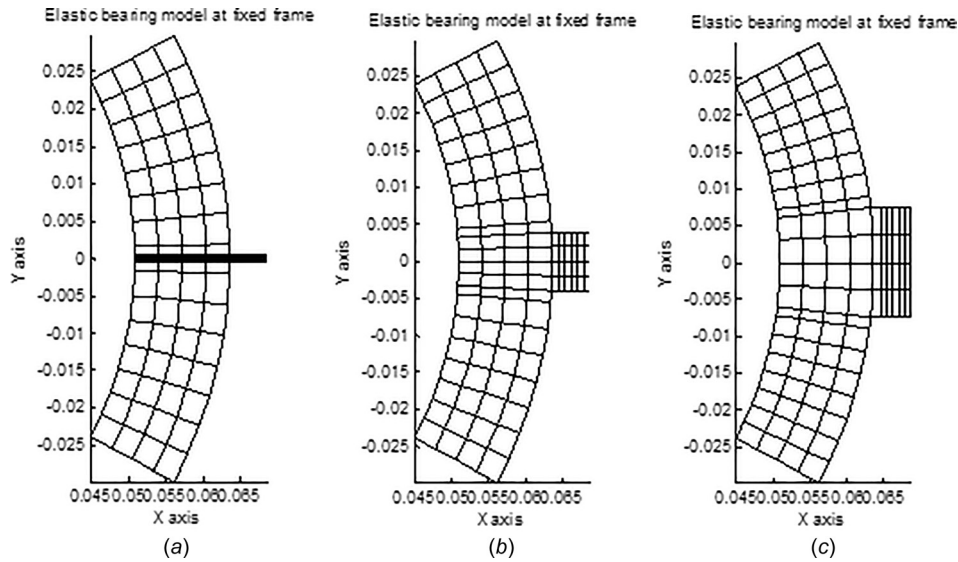


**Fig. 5 Pad-pivot FE model with different of web thicknesses: (a) 1 mm, (b) 8 mm, and (c) 15 mm**

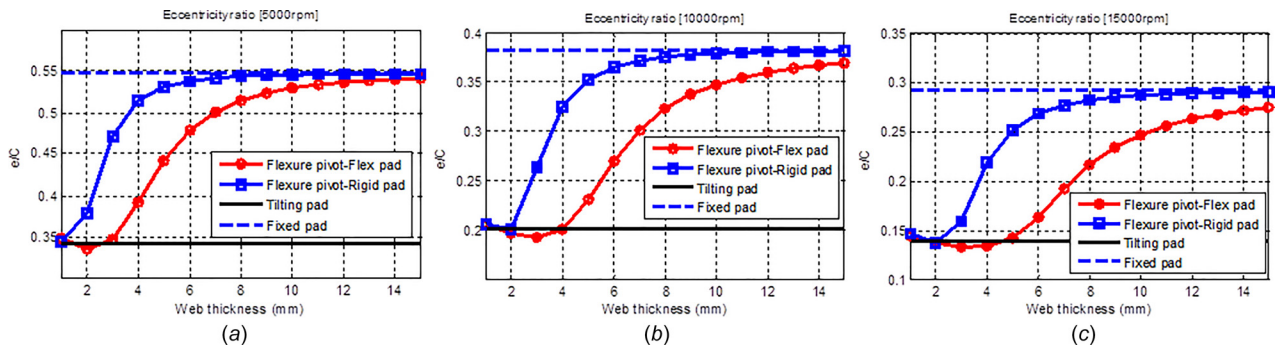


**Fig. 6 Journal eccentricity ratio with varying web thickness: (a) 5000 rpm, (b) 10,000 rpm, and (c) 15,000 rpm**

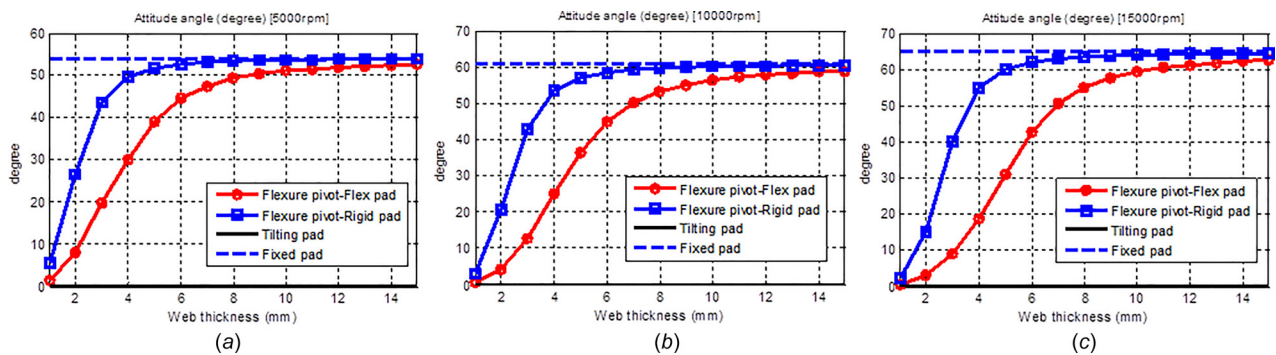


**Fig. 7 Journal attitude angle with varying web thickness: (a) 5000 rpm, (b) 10,000 rpm, and (c) 15,000 rpm**

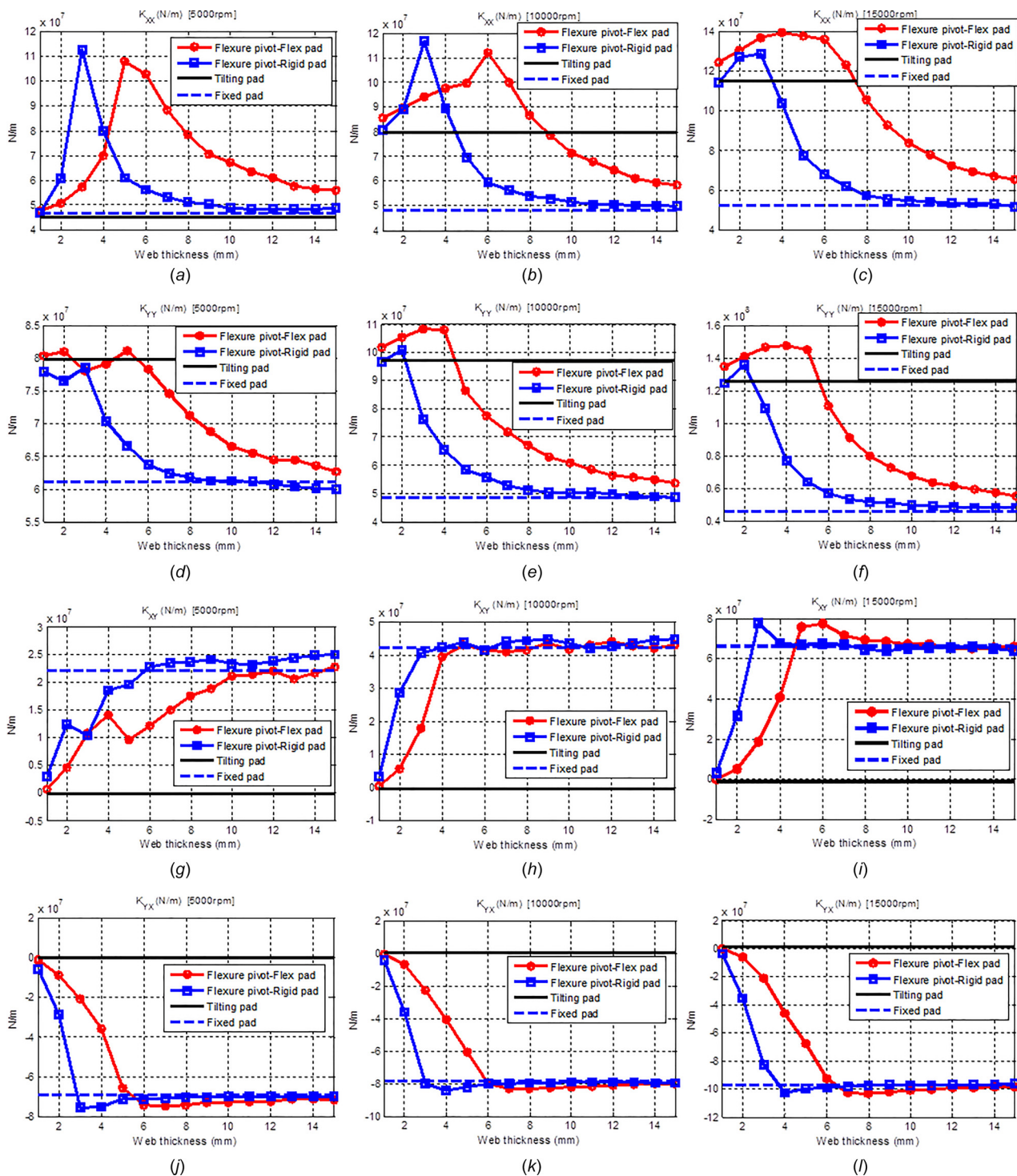
converge into the fixed pad bearing regime, where the rigid-pad FPJB produces a quicker response than the flexible pad model.

Figure 9 shows damping terms with the varying web thickness. As shown in the stiffness terms, rising and falling damping coefficients between 2 mm and 6 mm web thickness are observed except at  $c_{yy}$ . At the higher rotor spin speed, the abrupt variations are more clearly produced as seen in Fig. 9, where the rigid pad produces a faster convergence into the fixed-pad bearing properties.

The variation of the stiffness and damping coefficients with increasing pad tilt stiffness equivalent to the increasing web

thickness is provided by Armentrout and Paquette [6]. In the transient regime between the tilt pad and fixed geometry regimes, the abrupt changes of the dynamic properties observed in this research are also produced. San Andrés [8] provided the FPJB performance with the varying pivot rotational stiffness. The direct stiffness terms produced the rising and falling values in the transient area regardless of the exciting frequency.

Noticeable differences between the flexible pad-pivot and rigid-pad FPJB rotordynamic variables are shown in Figs. 7–9. The main differences between the two models are pad-pivot flexibility



**Fig. 8 Stiffness coefficients with varying web thickness: (a)  $k_{xx}$  at 5000 rpm, (b)  $k_{xx}$  at 10,000 rpm, (c)  $k_{xx}$  at 15,000 rpm, (d)  $k_{yy}$  at 5000 rpm, (e)  $k_{yy}$  at 10,000 rpm, (f)  $k_{yy}$  at 15,000 rpm, (g)  $k_{xy}$  at 5000 rpm, (h)  $k_{xy}$  at 10,000 rpm, (i)  $k_{xy}$  at 15,000 rpm, (j)  $k_{yx}$  at 5000 rpm, (k)  $k_{yx}$  at 10,000 rpm, and (l)  $k_{yx}$  at 15,000 rpm**

and the pivot modeling method. The flexible pad-pivot FE model utilizes a single body structure as shown in Fig. 5, whereas the rigid-pad model is identical to the rigid-pad TPJB model except for including an equivalent web-induced rotational stiffness.

In the case of the rigid-pad FPJB model, the tilting angle and the pivot radial deformation can be easily measured since the rotation center and the pivot position coincide; however, the flexible pad-pivot model does not provide any clear way for the evaluation of the pad-pivot angular and radial displacements. Figure 10

provides means to measure the equivalent tilting angle and web elastic deformation in the flexible-pad web FE model. The tilting motion takes place throughout the pad-web FE model as seen in Fig. 10(a). For simplicity, the tilting angle is measured in two different ways. Point A is fixed on the ground and point B would move in accordance with the pad-pivot elastic deformation. The straight line AB would be shifted to AB' with the pad tilt motion, and the angle between the two lines ( $\theta_{AB}$ ) can be considered as the tilt angle at the pivot location. On the other hand, two other

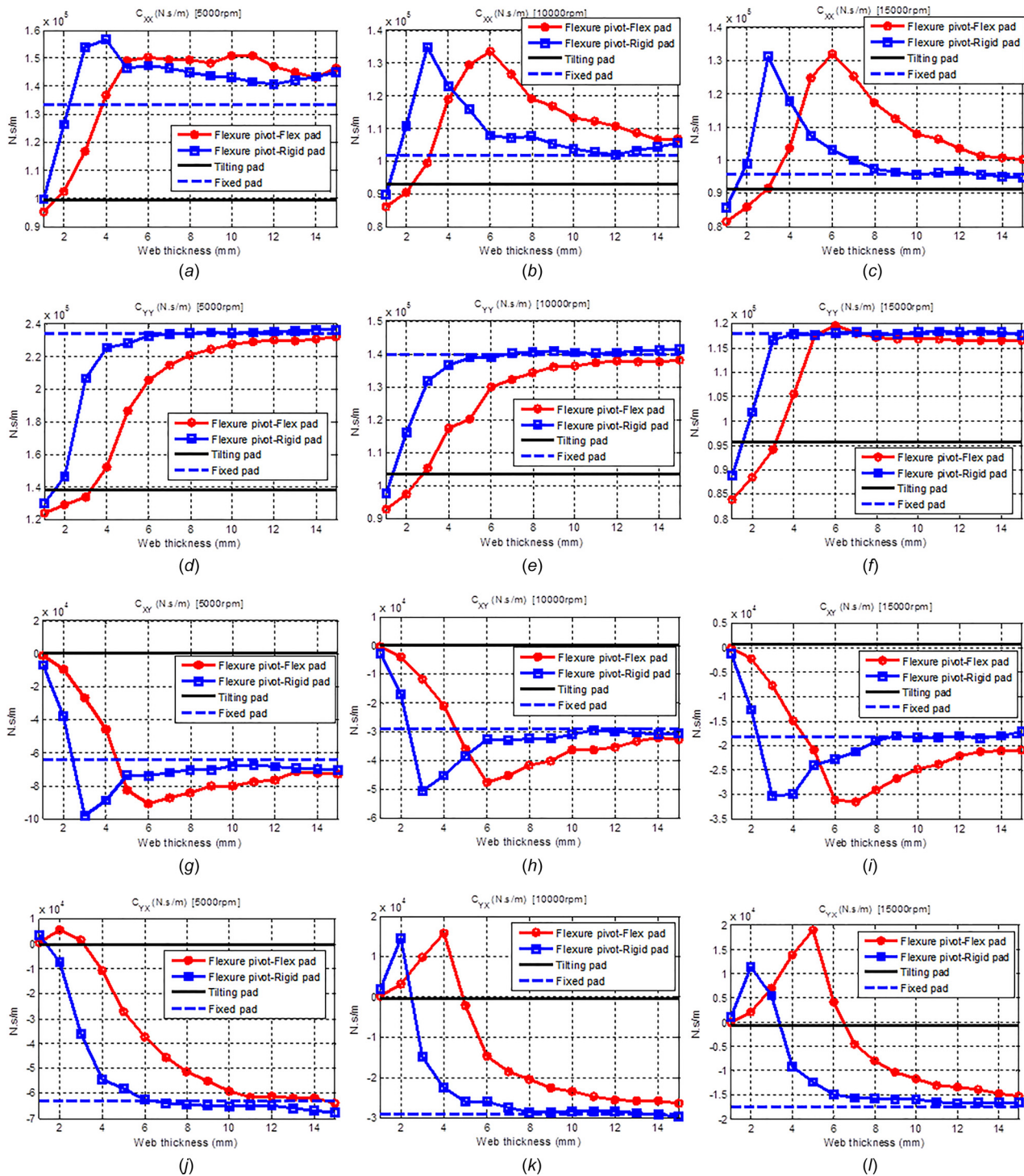


**Fig. 9 Damping coefficients with increasing web thickness: (a)  $c_{xx}$  at 5000 rpm, (b)  $c_{xx}$  at 10,000 rpm, (c)  $c_{xx}$  at 15,000 rpm, (d)  $c_{yy}$  at 5000 rpm, (e)  $c_{yy}$  at 10,000 rpm, (f)  $c_{yy}$  at 15,000 rpm, (g)  $c_{xy}$  at 5000 rpm, (h)  $c_{xy}$  at 10,000 rpm, (i)  $c_{xy}$  at 15,000 rpm, (j)  $c_{yx}$  at 5000 rpm, (k)  $c_{yx}$  at 10,000 rpm, and (l)  $c_{yx}$  at 15,000 rpm**

points (C and D) at the circumferential ends of the pad provide the information about the pad tilting angle. The positions of C and D would be shifted to  $C'$  and  $D'$  as seen in Fig. 10; hence, the angle between the two straight lines ( $\overline{CD}$  and  $\overline{C'D'}$ ) will provide the tilting angle ( $\theta_{CD}$ ). The two separate types of tilting angles ( $\theta_{AB}$  and  $\theta_{CD}$ ) will be simulated and discussed. Another useful way to investigate the differences between the two FPJB models is the pivot radial deformation. In the case of the rigid-pad FPJB model, the displacement of the pivot point becomes the pivot elastic deformation in the radial direction. In the case of the flexible

pad-pivot model, the difference between the line lengths ( $\overline{AB} - \overline{AB'}$ ) produces the pivot radial deformation.

The simulation results of two different types of tilting angles and the pivot radial deformation discussed in this section are depicted in Figs. 11 and 12, respectively. Simulation results for pads 1, 2, and 3 shown in Fig. 2 are provided since the attitude angle increase in a counter-clockwise manner with increased web thickness, and the resulting bearing loads are higher on the right side pads. Figures 11(a), 11(b), and 11(c) show the tilt angle of pad 1 at rotor spin speed of 5000, 10,000, and 15,000 rpm,

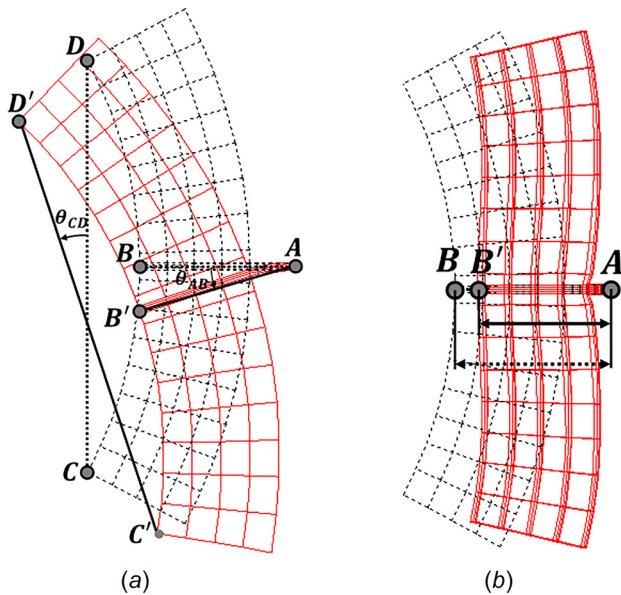


**Fig. 10** Tilting angle and pivot radial deformation (dotted line: original shape and bold line: deformed shape): (a) Pivot and web tilting angle and (b) pivot radial deformation

respectively. At the thinnest web (1 mm), rigid-pad model shows the largest tilting angle; however, the flexible pad-pivot model produces the larger values with increased web thickness. The other pads (2 and 3) provide the similar trends as shown in Figs. 11(d)–11(i), which means that the equivalent pivot stiffness model overpredicts the rotational stiffness leading to the smaller tilt angle. Tilting angle measured at the pad ( $\theta_{CD}$ ) is larger than at the pivot location ( $\theta_{AB}$ ). This means that the pad elastic deformation causes additional tilt motion. In another words, the pivot tilt angle measured by the pad-pivot elastic deformation ( $\theta_{CD}$ , see Fig. 10) is larger than the tilt angle measured only at the pivot location ( $\theta_{AB}$ ).

Normalized pad-pivot radial deformation with respect to bearing clearance ( $C_b$ ) is shown in Fig. 12. The dotted line indicates the flexible pad-pivot model, and the bold line is the rigid-pad model. In the case of the rigid-pad model, the web radial deformation is the radial displacement of the pivot location with the equivalent stiffness model. On the other hand, the radial deformation of the flexible pad-pivot model involves both pad and web elastic deformation as shown in Fig. 10(b). This may cause a larger amount of radial deformation in the flexible pad-web model. The equivalent web stiffness for both the pivot rotational and radial springs is seen to be overly stiff. The main reason for the noticeable difference of the static and dynamic properties seems to result

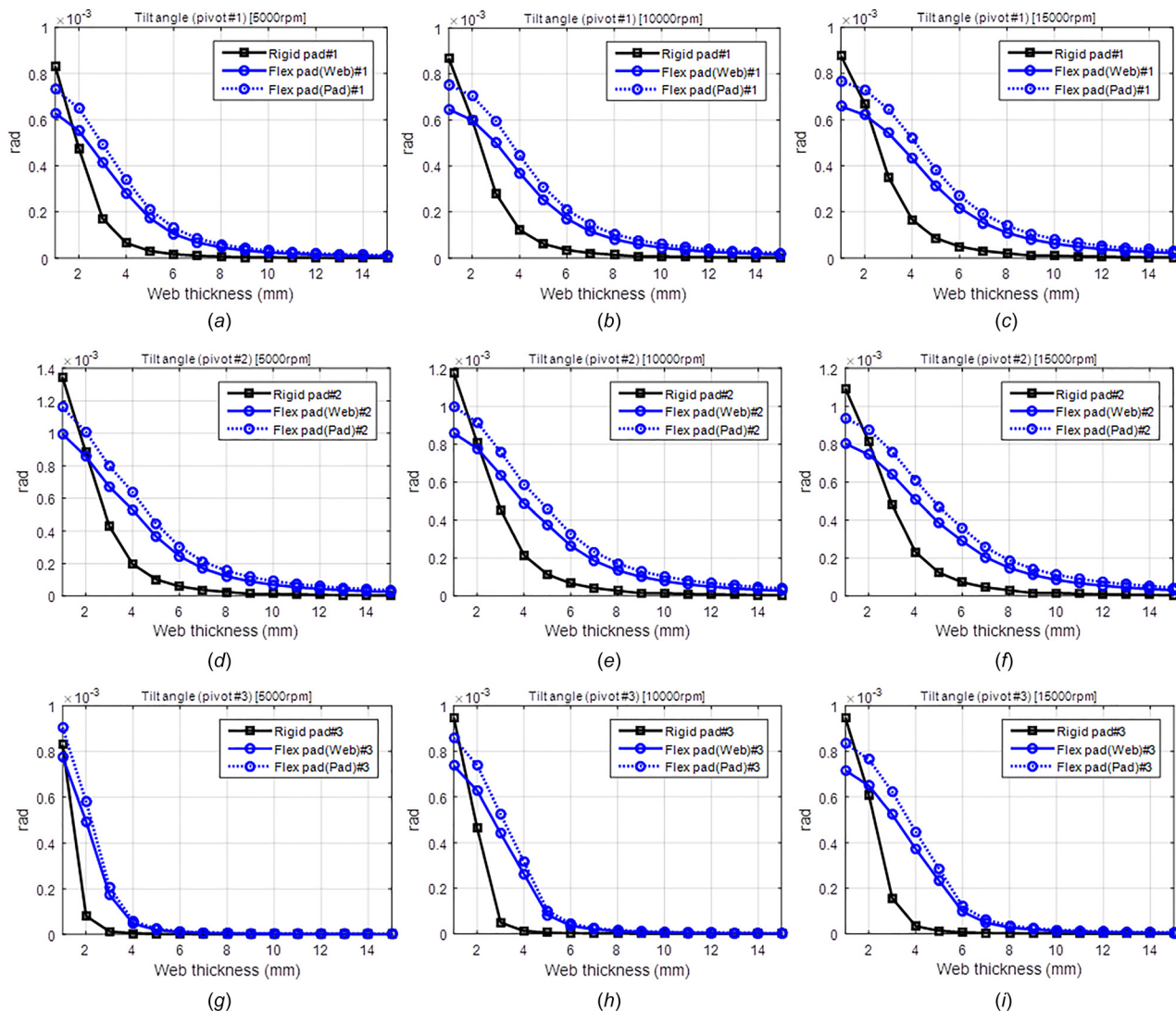


**Fig. 11** Tilting angle: (a) 5000 rpm (pivot #1), (b) 10,000 rpm (pivot #1), (c) 15,000 rpm (pivot #1), (d) 5000 rpm (pivot #2), (e) 10,000 rpm (pivot #2), (f) 15,000 rpm (pivot #2), (g) 5000 rpm (pivot #3), (h) 10,000 rpm (pivot #3), and (i) 15,000 rpm (pivot #3)

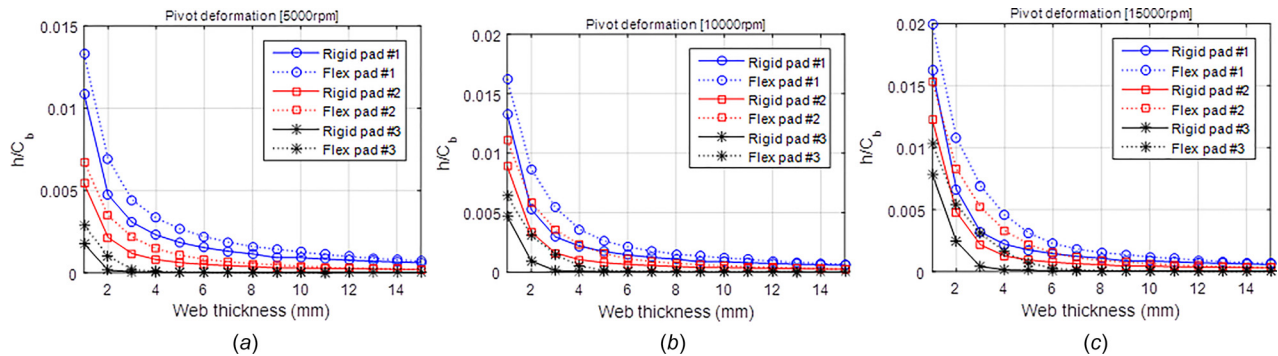


Fig. 12 Pivot radial deformation ratio: (a) 5000 rpm, (b) 10,000 rpm, and (c) 15,000 rpm

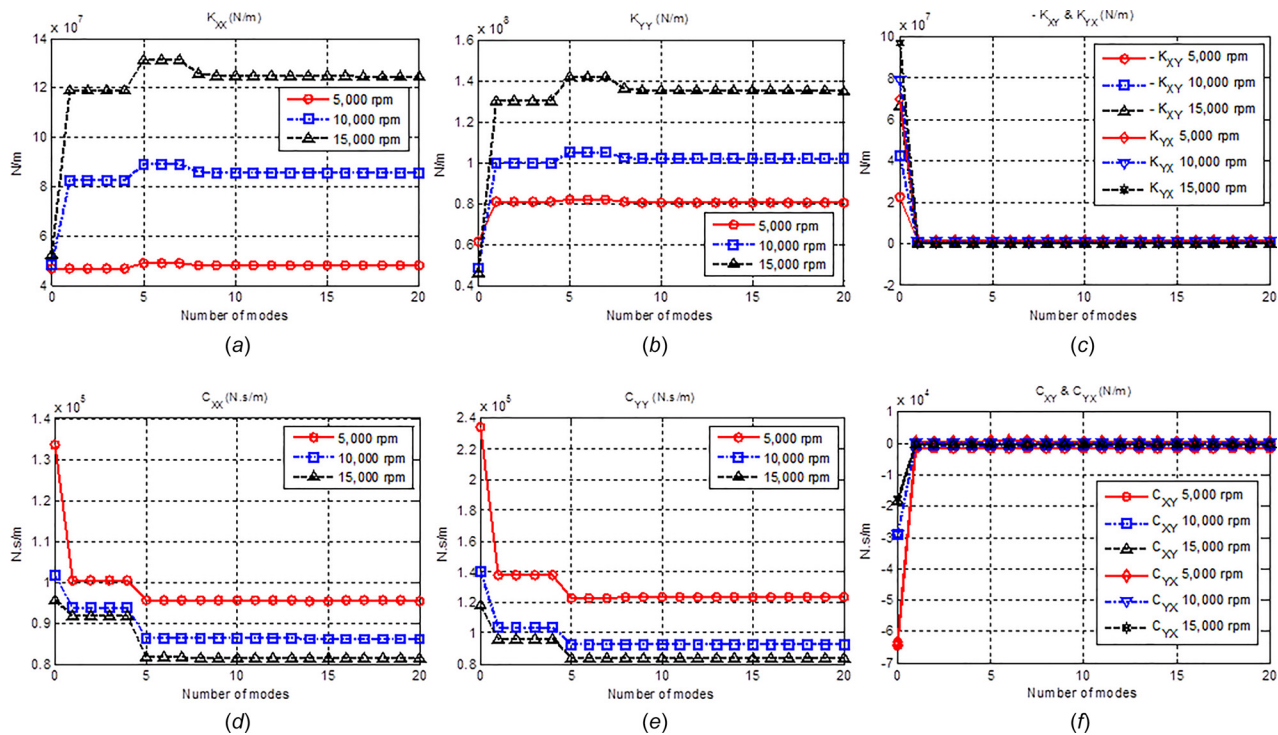


Fig. 13 Dynamic coefficients with varying number of modes: (a)  $k_{xx}$ , (b)  $k_{yy}$ , (c)  $k_{xy}$  and  $k_{yx}$ , (d)  $c_{xx}$ , (e)  $c_{yy}$ , and (f)  $c_{xy}$  and  $c_{yx}$

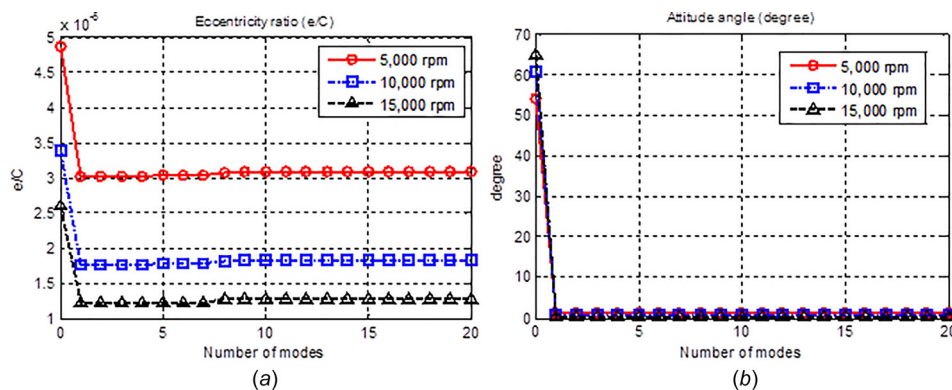
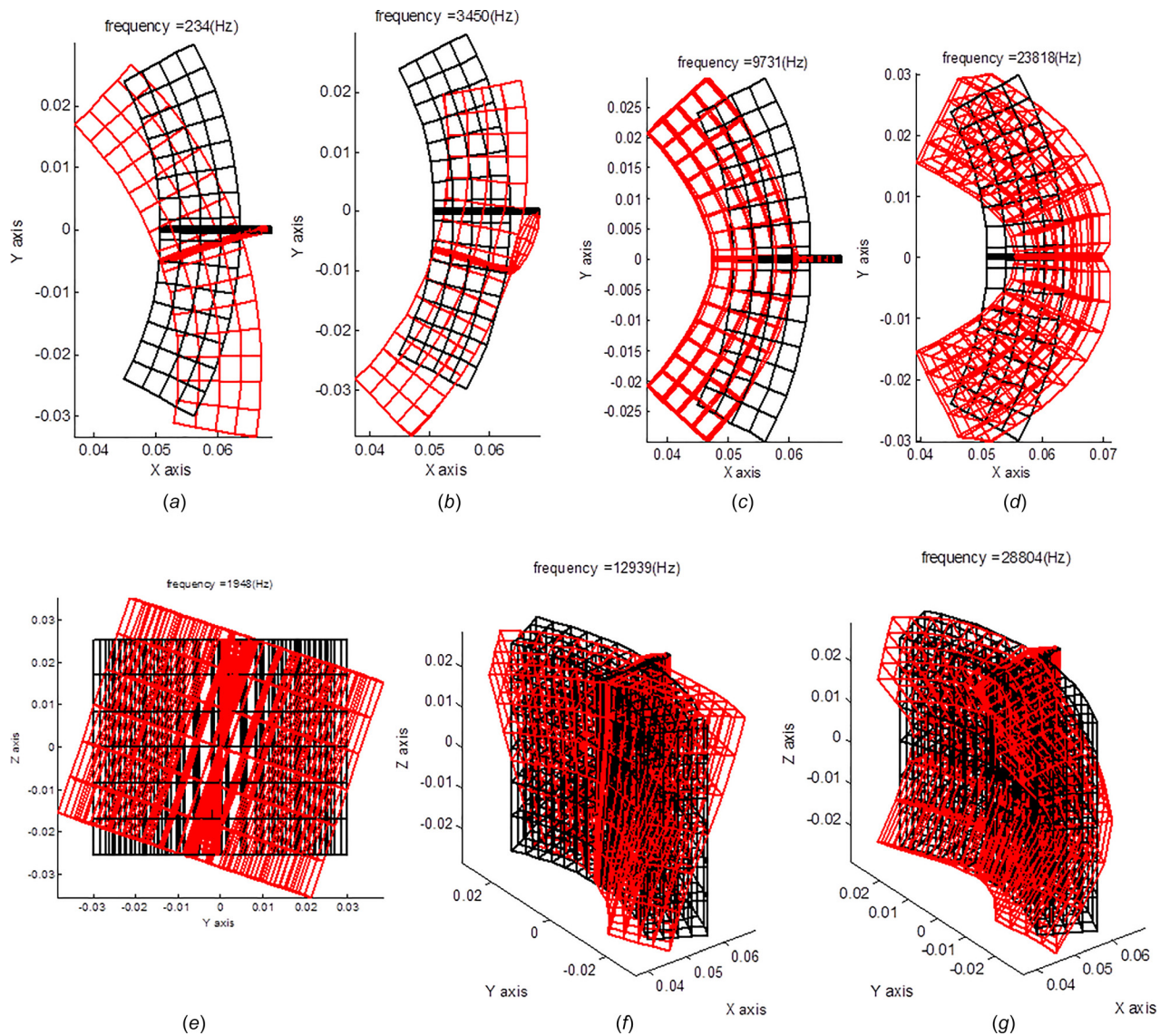


Fig. 14 Static characteristics with varying number of modes: (a) Eccentricity ratio and (b) attitude angle



**Fig. 15 Mode shapes: (a) first mode, (b) third translational mode, (c) fifth bending mode, (d) eighth bending mode, (e) second torsional mode, (f) seventh mode, and (g) ninth mode**

**Table 2 Flexure pivot bearing simulation parameters [10]**

Load configuration	LBP
Number of pads	4
Pad arc length (deg)	72
Offset	0.5
Radius of shaft (m)	0.0584
Bearing clearance (m)	$19.05 \times 10^{-5}$
Preload	0.25
Bearing length (m)	0.0762
Young's modulus (Pa) (assumed)	$2.10 \times 10^{11}$
Poisson's ratio (assumed)	0.3
Web thickness (m)	$21.251 \times 10^{-5}$
Web height (m)	$743.79 \times 10^{-5}$
Pad thickness (m) (assumed)	$12.7 \times 10^{-3}$
Lubricant	ISO VG32 turbine
Rotor spin speed (rpm)	4000, 6000, 8000, 10,000, 12,000
Unit load (kPa)	348.4, 1038.2

from the effect of the overpredicted pivot stiffness on the pad tilt angles and the pivot radial deformations [7].

As shown in the simulation results of the static and dynamic properties, the flexible pad-web FE model produces noticeably different results from the rigid-pad model. The difference between the static and dynamic properties between the rigid- and flexible-pad FPJBs varies depending on the rotor spin speed or other running conditions. The bearing designer should choose the optimum web thickness in accordance with the system configurations. As seen with the stiffness coefficients, the rigid-pad model produces a faster convergence as the web thickness increases. The flexible pad-pivot FE model provides more realistic dynamic behavior, and the noticeable differences between the rigid- and flexible-pad models indicate that the conventional methods using a rigid-pad model will produce overpredicted pivot rotational stiffness.

**3.2 Number of Modes.** In Sec. 3.1, both static and dynamic characteristics of FPJB were simulated, and compared to the fixed pad and tilting pad journal bearing models to investigate the web thickness effects. Twenty lower eigenmodes are taken into account to produce the flexible pad-pivot behavior. Suh and Palazzolo [21] examined the eigenmodes effects on the TPJB static and

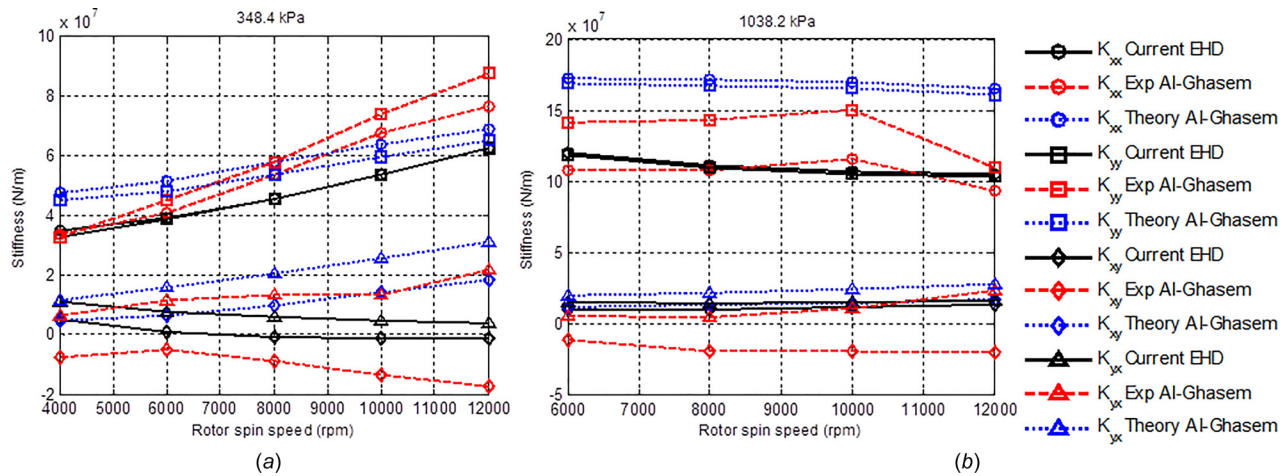


Fig. 16 Stiffness coefficients versus rotor speeds for different bearing unit load: (a) 348.4 kPa and (b) 1038.2 kPa

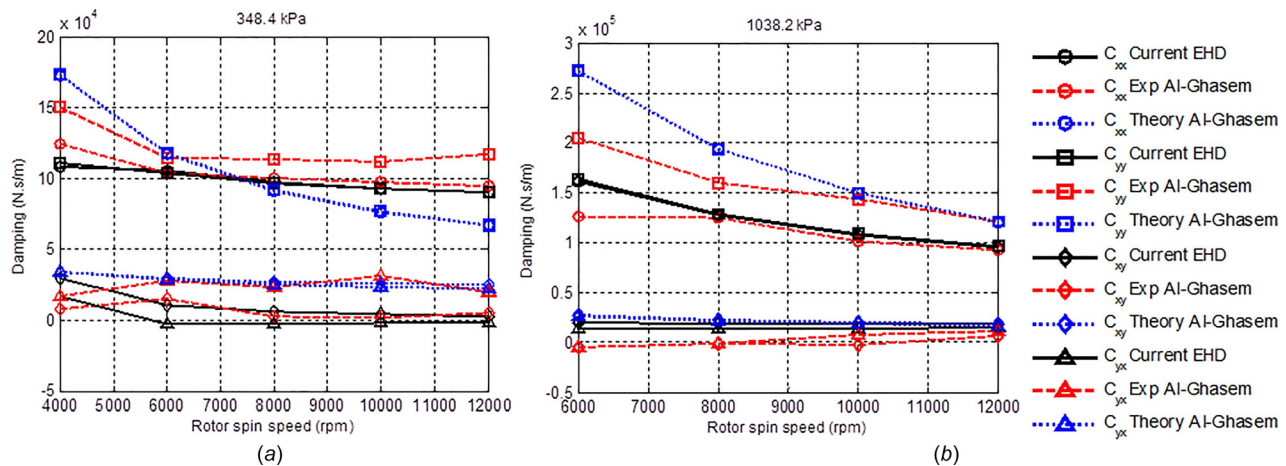


Fig. 17 Damping coefficients versus rotor speeds for different bearing unit load: (a) 348.4 kPa and (b) 1038.2 kPa

dynamic behaviors by gradually increasing the number of modes. An increased number of eigenmodes can produce more realistic pad-pivot behavior and will provide more accurate simulation results; however, the computation time may increase significantly. Judicious selection of a small set of lower “governing” modes will enable the computation time to become dramatically decreased while maintaining high accuracy. In this section, number of eigenmodes will be increased based on the eigenvalue frequency while examining the static and dynamic characteristics. Figure 13 provides bearing dynamic coefficients, and Fig. 14 shows the static properties. When the number of mode becomes zero on  $x$ -axis as shown in Figs. 13 and 14, FPJB produces rigid bearing behavior since the flexible pad-pivot FE model does not provide any dynamic motion.

Including the first mode, abruptly change every static and dynamic characteristic. Other modes producing a noticeable change are fifth and eighth modes. For example, the  $x$ -axis of five on Fig. 13 means that the five lowest eigenvectors of the elastic pad-pivot FE model are taken into account to express the pad-pivot elastic deformation. Several eigenmodes are depicted in Fig. 15. The first mode causing this abrupt initial change is the tilting mode, which is the main reason for the use of the FPJB. This tilting motion includes not only the pad tilting but also a sliding motion in the circumferential direction. A pure translational motion in the circumferential direction can be seen in the third mode, which does not make any noticeable effects on the static and dynamic behavior of the FPJB. The fifth mode is the pad bending mode, which makes the biggest influence on FPJB

properties except the first bending mode. Suh and Palazzolo [21] found that the first bending mode of the pad changes both direct stiffness and damping terms. According to Suh and Palazzolo’s research [21], the first bending mode increased the direct stiffness terms and decreased damping terms in EHD model, which is the same result as in this research. In TEHD model, the first bending mode decreased the direct stiffness and damping terms. Another governing mode is the eighth mode, bending mode at a higher frequency including the web radial deformation. The rigid-pad FPJB model in this research considered the rotational and radial stiffness, and the stiffness in circumferential direction is ignored, which is a good assumption according to the flexible pad-pivot simulation results.

**3.3 Comparison to Experimental Results.** The newly developed FPJB model is compared with the experimental work and numerical result predicted by the bulk-flow model of Al-Ghasem and Childs [10]. The simulation results provided in this section are limited to the synchronously reduced dynamic coefficients, and the frequency dependency is ignored. The bearing input parameters for the simulation are shown in Table 2. Two different unit load cases (348.4 kPa, 1038.2 kPa) are simulated from 4000 rpm to 12,000 rpm for unit load of 348.4 kPa, and from 6000 rpm to 12,000 rpm for the unit load of 1038.2 kPa. Pad’s thickness, Young’s modulus, and Poisson’s ratio are assumed since they are not provided in the Al-Ghasem and Childs’ research paper [10]. Stiffness coefficients with varying rotor spin speed are

shown in Fig. 16. In the 384.4 kPa unit loading case, the current numerical FPJB model (flexible pad-pivot FE model) predicted lower direct stiffness than the test result [10] except for the 4000 rpm case. The bulk-flow model [10] is less sensitive to increasing rotor spin speed than the test result and the current model. In the 1038.2 kPa unit loading case, the direct stiffness terms are overestimated by the bulk-flow model over the full rotor spin speed range. The absolute values of the predicted cross coupled terms are also lower than the test results and the bulk-flow model.

The damping coefficients for both 348.4 kPa and 1038.2 kPa unit load cases are compared in Fig. 17. In the 348.4 kPa unit loading case, the bulk-flow model [10] is more sensitive to the increasing rotor spin speed than the test result and the current model. The current research predicted lower direct damping terms in the 348.4 kPa unit load case. In the 1038.2 kPa case, both direct damping terms of the current model are located between two direct damping terms of the experimental results over all the spin speed range as shown in Fig. 17. In the case of the cross coupled damping terms, the absolute values of the current numerical model are underestimated in the 348.4 kPa unit load case and overpredicted in the 1038.2 kPa case.

#### 4 Conclusion

This study presented a new modeling method and algorithm for the evaluation of the static and dynamic characteristics of the flexible pad-pivot FPJB, adopting nonlinear transient dynamic analysis. This study can be summarized as follows:

- (a) Modal coordinate transformation is included for calculating the flexible pad-pivot dynamic behavior, in order to increase computational efficiency.
- (b) Flexible pad-pivot FE model was simulated and compared to the rigid-pad FPJB, fixed-pad bearing and TPJB with varying web thickness.
- (c) Static and dynamic characteristics of the FPJB were simulated with varying number of eigenmodes of the flexible pad-pivot FE model. The fifth bending mode except the first tilting mode, was found to have the biggest influence on the FPJB properties.
- (d) Both rigid-pad analytical FPJB and flexible pad-pivot FPJB FE models were simulated with fifteen different web thickness (1–15 mm) converging into the fixed-pad bearing static and dynamic properties. The flexible pad-pivot model produced slower convergence rate with increasing web thickness, which means the conventional approach with the rigid-pad FPJB model will have difficulty in accurately predicting static and dynamic bearing performance.

#### Acknowledgment

The authors gratefully acknowledge the support of this research from the Texas A&M Turbomachinery Research Consortium (TRC) member companies.

#### Nomenclature

- $f_{E-PW-FL}$  = modal force vector acting on elastic pad FE model  
 $F_{E-PW-FL}$  = fluid load on elastic pad FE model  
 $F_{SHFT}$  = force vector acting on the spinning journal  
 $h_n$  =  $n$ th nodal film thickness  
 $j_n$  =  $n$ th nodal point on journal  
 $k_{E-PW}$  = modal stiffness of elastic pad-pivot FE model  
 $K_{E-PW}$  = stiffness matrix of elastic pad-pivot FE model  
 $m_{E-PW}$  = modal mass of elastic pad-pivot FE model  
 $M_{E-PW}$  = mass matrix of elastic pad-pivot FE model

- $p$  = fluid pressure  
 $p_n$  =  $n$ th nodal point on pad  
 $R_n$  = journal radius  
 $t_{EDYN}$  = user-defined end time of the numerical simulation  
 $U$  = shaft surface linear velocity  
 $X_{E-PW}$  = nodal displacement vector of elastic pad-pivot FE model  
 $Y_{OE-PW}$  = initial states of flexible pad-pivot  
 $Y_{OSHFT}$  = initial states of journal  
 $Z_{E-PW}$  = modal displacement vector of elastic pad-pivot FE model  
 $\mu$  = fluid viscosity  
 $\omega$  = journal spin speed  
 $\Phi_{E-PW}$  = eigenvector of elastic pad-pivot FE model

#### References

- [1] Lund, J. W., 1964, "Spring and Damping Coefficients for the Tilting-Pad Journal Bearing," *ASLE Trans.*, **7**(4), pp. 342–352.
- [2] Nilsson, L., 1978, "The Influence of Bearing Flexibility on the Dynamic Performance of Radial Oil Film Bearings," 5th Leeds-Lyon Symposium on Tribology, Lyon, France, pp. 19–22.
- [3] Lund, J. W., and Pedersen, L. B., 1987, "The Influence of Pad Flexibility on the Dynamic Coefficients of a Tilting Pad Journal Bearing," *ASME J. Tribol.*, **109**(1), pp. 65–70.
- [4] Earles, L. L., Palazzolo, A. B., and Armentrout, R. W., 1990, "A Finite Element Approach to Pad Flexibility Effects in Tilt Pad Journal Bearings: Part I—Single Pad Analysis," *ASME J. Tribol.*, **112**(2), pp. 169–176.
- [5] Desbordes, H., Fillon, M., Frêne, J., and Wai, C. C. H., 1995, "The Effects of Three-Dimensional Pad Deformations on Tilting-Pad Journal Bearings under Dynamic Loading," *ASME J. Tribol.*, **117**(3), pp. 379–384.
- [6] Armentrout, R. W., and Paquette, D. J., 1993, "Rotordynamic Characteristics of Flexure-Pivot Tilting-Pad Journal Bearings," *Tribol. Trans.*, **36**(3), pp. 443–451.
- [7] Chen, W. J., 1995, "Bearing Dynamic Coefficients of Flexible-Pad Journal Bearings," *Tribol. Trans.*, **38**(2), pp. 253–260.
- [8] San Andres, L., 1996, "Turbulent Flow, Flexure-Pivot Hybrid Bearings for Cryogenic Applications," *ASME J. Tribol.*, **118**(1), pp. 190–200.
- [9] Walton, N. V., and San Andres, L., 1997, "Measurements of Static Loading Versus Eccentricity in a Flexure-Pivot Tilting Pad Journal Bearing," *ASME J. Tribol.*, **119**(2), pp. 297–304.
- [10] Al-Ghaseem, A. M., and Childs, D. W., 2006, "Rotordynamic Coefficients Measurements Versus Predictions for a High-Speed Flexure-Pivot Tilting-Pad Bearing (Load-Between-Pad Configuration)," *ASME J. Eng. Gas Turbines Power*, **128**(4), pp. 896–906.
- [11] Rodriguez, L. E., and Childs, D. W., 2006, "Frequency Dependency of Measured and Predicted Rotordynamic Coefficients for a Load-on-Pad Flexible-Pivot Tilting-Pad Bearing," *ASME J. Tribol.*, **128**(2), pp. 388–395.
- [12] Hensley, J. E., and Childs, D., 2008, "Measurements Versus Predictions for Rotordynamic Characteristics of a Flexure Pivot-Pad Tilting Pad Bearing in an LBP Condition at Higher Unit Loads," *ASME Paper No. GT2008-50066*.
- [13] Kepple, W. E., Read, D. W., Zeidan, F. Y., Paraskevacos, C., and Dawson, M. P., 1998, "Experience in the Use of Flexure Pivot Tilt Pad Bearings in Boiler Feed Water Pumps," 15th International Pump User Symposium provide link for [15th International Pump User Symposium](#), Texas A&M University, College Station, TX, Mar. 3–5, pp. 77–84.
- [14] Pettinato, B. C., and De Choudhury, P., 2002, "Rotordynamic Tests of a Flexible Rotor on Flexure Pivot Journal Bearings and Stability Correlation With Frequency Dependent Characteristics," *31st Turbomachinery Symposium*, Texas A&M University, College Station, TX, pp. 39–47.
- [15] Kim, J., Palazzolo, A., and Gadangi, R., 1995, "Dynamic Characteristics of TEHD Tilt Pad Journal Bearing Simulation Including Multiple Mode Pad Flexibility Model," *ASME J. Vib. Acoust.*, **117**(1), pp. 123–135.
- [16] Boedo, S., and Booker, J. F., 1997, "Surface Roughness and Structural Inertia in a Mode-Based Mass-Conserving Elastohydrodynamic Lubrication Model," *ASME J. Tribol.*, **119**(3), pp. 449–455.
- [17] Boedo, S., and Booker, J. F., 2000, "A Mode-Based Elastohydrodynamic Lubrication Model With Elastic Journal and Sleeve," *ASME J. Tribol.*, **122**(1), pp. 94–102.
- [18] Boedo, S., and Booker, J. F., 2001, "Finite Element Analysis of Elastic Engine Bearing Lubrication: Theory," *Rev. Eur. Éléém.*, **10**(6–7), pp. 705–724.
- [19] Boedo, S., and Booker, J. F., 2001, "Finite Element Analysis of Elastic Engine Bearing Lubrication: Application," *Rev. Eur. Éléém.*, **10**(6–7), pp. 705–724.
- [20] Boedo, S., and Booker, J. F., 2005, "Modal and Nodal EHD Analysis for Gas Journal Bearings," *ASME J. Tribol.*, **127**(2), pp. 306–314.
- [21] Suh, J. H., and Palazzolo, A., 2015, "Three-Dimensional Dynamic Model of TEHD Tilting-Pad Journal Bearing—Part I: Theoretical Modeling," *ASME J. Tribol.*, **137**(2), p. 041703.
- [22] Cook, R. D., 1994, *Finite Element Modeling for Stress Analysis*, Wiley, New York.